scientific reports

Check for updates

OPEN

Ab-initio Study of structural, elastic, electronic and optical properties of hexahalometallate single crystals K_2XBr_6(X = Se, Pt)

Y. Naceur[1], H. Bourbaba[1], M. A. Ghebouli[2,3], L. Krache[4], B. Ghebouli[5], T. Chihi[3], M. Fatmi[3]✉ & Sultan Alomairy[6]

Some physical properties of hexahalometallate K_2XBr_6(X = Se, Pt) were computed in the zinc blend structure using GGA-PBESOL. The cell constant of K_2SeBr_6 and K_2PtBr_6 is consistent to the experiment value quoted in the literature, where the error is 0.95% and 1%. K_2SeBr_6 and K_2PtBr_6 present covalent bonding, high anisotropy and are ductile. The elastic constants of K_2SeBr_6 and K_2PtBr_6 are significantly smaller due to their larger reticular distances, lower Coulomb forces and then they are soft and damage tolerant. The interatomic separation is greater in K_2SeBr_6 than in K_2PtBr_6, hence the Coulomb interaction in K_2PtBr_6 is greater than that of K_2SeBr_6. The internal coordinate of Br atom in K_2PtBr_6 is lower than that of the same atom in K_2SeBr_6, and this can be explained by the fact that it is inversely proportional to the atom radius of Se and Pt. There are two major plasmonic processes, with intensities 3.7 and 1.35 located around 53.5 nm and 72.8 nm for K_2SeBr_6 and K_2PtBr_6.

Progress in experiment and theory, coupled with computational model is accelerating the discovery of new materials with useful physical parameters. The cubic antifluorite class K_2XBr_6(X = Pt, Se) have received increased interest since they exhibit structural phase transitions at lower temperatures. The family of hexahalometallate attracts researchers due to their light-absorbing materials in photovoltaic applications. The hexahalometallate double perovskites K_2XBr_6(X = Pt, Se) crystallize in the cubic antifluorite K_2PtCl_6 structure. They have the stoichiometric formula X_2MA_6, where X, M and A are alkaline metal, polyvalent or heavy transition metal and halogen. The K atom in K_2XBr_6 (X = Pt, Se) of the three-dimensional structure is bonded to twelve equivalents Br atoms to form KBr12 cuboctahedra. The faces contain six equivalents KBr12 cuboctahedra and four equivalents PtBr6 (SeBr6) octahedral. Studies conducted by other researchers, it is stated that, the investigation on elastic constants and compressibility of K_2XBr_6(X = Pt, Se) has carried out experimentally by N. Wruk et al. using Brillouin scattering and ultrasonic wave velocity measurements[1]. The study conducted by Walter Abriel and Mary Anne White on K_2SeBr_6 by x-ray powder diffraction in the temperature range 10 K to 290 K, and heat capacity measurements indicates three phases for K_2SeBr_6, K_2PtCl_6 cubic structure, Rb_2TeI_6 tetragonal structure and K_2TeBr_6 monoclinic structure[2]. The phase-transition temperatures of hexahalometallate material K_2PtBr_6 (K_2SeBr_6) have been studied experimentally and found to be 209 K, 221 K and 249 K[1] (78 K, 105 K, 137 K, 143 K and 169 K[1]). K_2XBr_6(X = Pt, Se) hexahalometallate materials show a suitable energy gap, sufficient absorption, low reflectivity, weaker cost and therefore adequate performance for photovoltaic applications[3–7]. Our study confirms the characteristics of mentioned materials above, which have a band gap range of (0.98 eV to 2.25 eV), an absorption coefficient of 237,311 cm^{-1} (211,556 cm^{-1}) and reflectivity of (0.1–0.3%) in the extreme ultraviolet light. The band gap range (1–2.25 eV) and the absorption of extreme ultraviolet light make K_2SeBr_6 and K_2PtBr_6 as absorber materials in solar cells. These compounds are poor reflector and can be used as an anti-reflection coating material.

The aim of this work is the use of GGA-PBESOL and HSE hybrid approximations to obtain adequate structural, elastic and optoelectronic properties of K_2XBr_6 (X = Pt, Se). The paper is organized such as the calculation

[1]LPDS University of Tahri Mohamed, 08000 Béchar, Algeria. [2]Department of Chemistry, Faculty of Technology, University of Mohamed Boudiaf, 28000 M'sila, Algeria. [3]Research Unit On Emerging Materials (RUEM), University Ferhat Abbas of Setif 1, 19000 Setif, Algeria. [4]PQSD Laboratory, Department of Physics, Faculty of Science, University Ferhat Abbas of Setif 1, 19000 Setif, Algeria. [5]Laboratory of Studies Surfaces and Interfaces of Solids Materials, Department of Physics, Faculty of Science, University Ferhat Abbas of Setif 1, 19000 Setif, Algeria. [6]Department of Physics, College of Science, Taif University, P.O. Box 11099, Taif 21944, Saudi Arabia. ✉email: fatmimessaoud@yahoo.fr

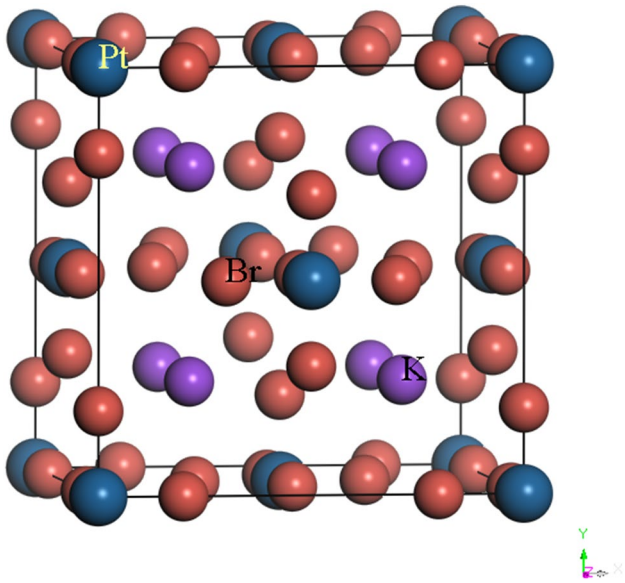

Figure 1. The crystal structure of K_2PtBr_6.

scheme is detailed in the second part. The exposure and discussion of obtained results are reported in the third section. This work is concluded by an conclusion in the last part.

Calculation scheme

Calculations were carried out using the DFT framework as implemented in the CASTEP code[8]. The valence states of K_2XBr_6(X = Se, Pt) are K: $4s^1$, Se: $4p^4$, Pt: $5d^9$ and Br: $4p^5$. An ultra soft pseudo-potential type Vanderbilt[9] describes the interaction of valence electrons and ions cores. The GGA-PBESOL of Perdew et al.[10] is adopted for the non-local correlation exchange effect. The best convergence of the computed structures and energies requires the use of cut-off energy of 630 eV. The irreducible Brillouin zone was sampled up to 8 × 8 × 8 k-grid on the Monkhorst–Pack scheme[11]. The tolerance of geometry optimization were a difference of total energy 5×10^{-6} eV/atom, a maximum ionic Hellmann–Feynman force 10^{-2} eV/Å, maximum stress 2×10^{-2} eV/Å^3 and ionic displacement of 5×10^{-4} Å. The calculation of the optical parameters requires the use of uniform distribution of 20 × 20 × 20 k-points. The self-consistent calculations converge if the total energy is minimal. The structural parameters were estimated using the minimization technique of Broyden-Fletcher-Goldfarb-Shanno (BFGS)[12], which provide a fast way to find the lowest energy structure. The basic idea behind the hybrid functionals is to mix exchange energies calculated in an exact (Hartree–Fock-like) manner with those obtained from DFT methods in order to improve performance. The accuracy of the electronic properties predicted by density functional theory depends on the used exchange–correlation functional. Non-local hybrid functionals gives more accurate results than semi-local functionals. The non-local Hartree–Fock exchange is an integral part of the hybrid functionals implemented in the FLAPW mehod[13]. The non-local exchange in HSE enlarges the elements of the optical transition matrix and leads to better accuracy of HSE in calculating electronic properties. Omitting the non-local exchange in the transition operator for HSE leads to errors. The importance of non-local correction in the velocity gauge has been widely discussed for non-local pseudo potentials[14,15]. The neglect of the non-local term in the velocity gauge leads to inaccuracy, especially for transitions that involve localized d electrons[16,17]. The non-locality of the potential comes from the fact that the electron Hamiltonian is replaced by an approximate Hamiltonian in the independent electron approximation with an effective potential, which reintroduces the electron–electron interactions in the Kohn–Sham equations.

Results and discussion

Structure and morphology. The crystal structure of K_2PtBr_6 is illustrated in Fig. 1. The location of atoms is such that (Se, Pt) atom is placed at the center of the octahedron formed by the four atoms of Br. The K atoms occupy interstitial sites. The antifluorite class K_2XBr_6(X = Se, Pt) adopt the cubic structure with space group Fm3m at ambient conditions. The occupied Wyckoff sites for K, (Se, Pt) and Br atoms are ± (1/4, 1/4, 1/4) a_0, (0, 0, 0) a_0 and ± (x, 0, 0) a_0, ± (0, x, 0) a_0 , ± (0, 0, x) a_0. The lattice constant, bulk modulus and its pressure derivative of K_2XBr_6(X = Se, Pt) are listed in Table 1. The cell constant of K_2SeBr_6 and K_2PtBr_6 is consistent to the experimental value quoted in the literature[1,2], where the error is 0.95% and 1%. The bulk modulus calculated for K_2SeBr_6 and K_2PtBr_6 using the fit scheme $P(V/V_0)$ as reported in Fig. 2 is in good agreement with available experimental data[1]. The interatomic distances d_{X-Br}, d_{K-Br} and d_{Br-Br} in K_2SeBr_6 (K_2PtBr_6) at equilibrium are 2.5681 Å, 3.6769 Å and 3.6319 Å (2.4703 Å, 3.6306 Å and 3.4936 Å). It should be pointed that, bond lengths reported for K_2SeBr_6 are in good agreement with those found in the literature $d_{Se-Br} = 2.555$ Å, $d_{Pt-Br} = 2.50$ Å, $d_{K-Br} = 3.685$ Å and $d_{Br-Br} = 3.613$ Å[2]. Figure 3 shows the effect of pressure on d_{K-Br}, d_{Br-Br} and d_{Br-X} (X = Se, Pt) bond lengths in K_2SeBr_6 and K_2PtBr_6. The bond lengths in K_2SeBr_6 are large than those in K_2PtBr_6; hence, the

	K_2SeBr_6			K_2PtBr_6		
	This Work	Experiment	Other	This Work	Experiment	Other
A (Å)	10.2653	10.363 [1]		10.3995	10.293 [1]	
x	0.24065			0.24695		
$^*B_0$ (GPa)	15.35	16.70 [1]		15.43	15.20 [1]	
B'	6.15			7.20		
C_{11} (GPa)	15.49	23.20 [1]		22.27	21.60 [1]	
C_{12} (GPa)	11.95	13.50 [1]		8.97	12.0 [1]	
C_{44} (GPa)	7.08	9.30 [1]		5.95	8.50 [1]	
$^{**}B_0$ (GPa)	13.13			13.40		

Table 1. The lattice constant, bulk modulus and its pressure derivative and elastic moduli of K_2XBr_6(X = Se, Pt).

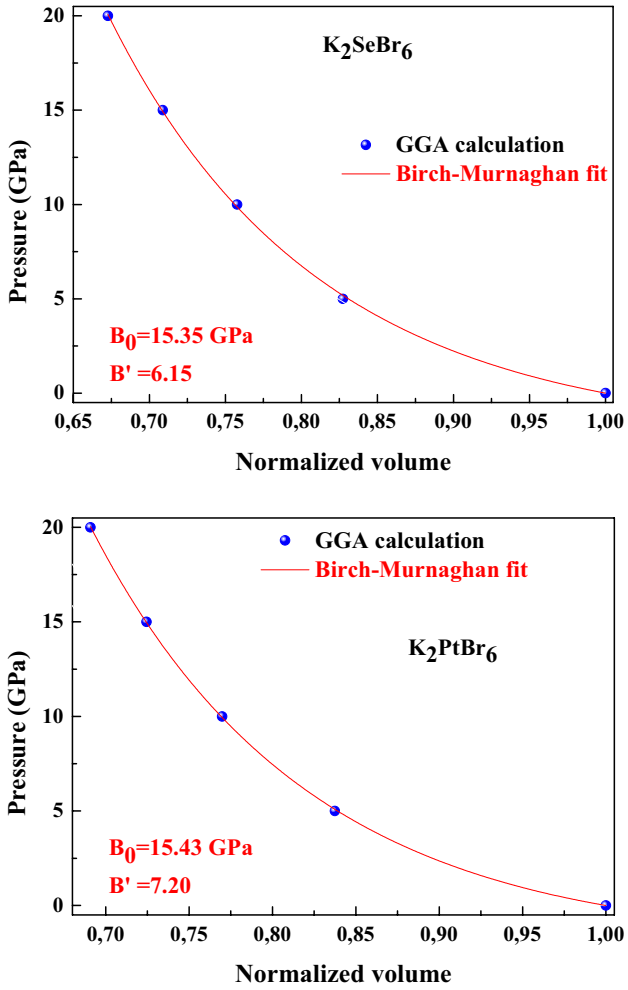

Figure 2. The pressure effect on normalized volume in K_2SeBr_6 and K_2PtBr_6.

Coulomb interaction in K_2PtBr_6 is greater than that in K_2SeBr_6, which can be explained by the fact that the distances are inversely proportional to the lattice constant. Also, the distance $d_{Br\text{-}Se}$ is greater than that of $d_{Br\text{-}Pt}$. All bond lengths decrease monotonously when the pressure increases. Figure 4 displays the effect of pressure on the internal coordinate of Br atom in K_2SeBr_6 and K_2PtBr_6. The internal coordinate of Br atom in K_2PtBr_6 is lower than that of the same atom in K_2SeBr_6, and this is explained by the fact that it is inversely proportional to the atom radius of Se (1.15 Å) and Pt (1.35 Å).

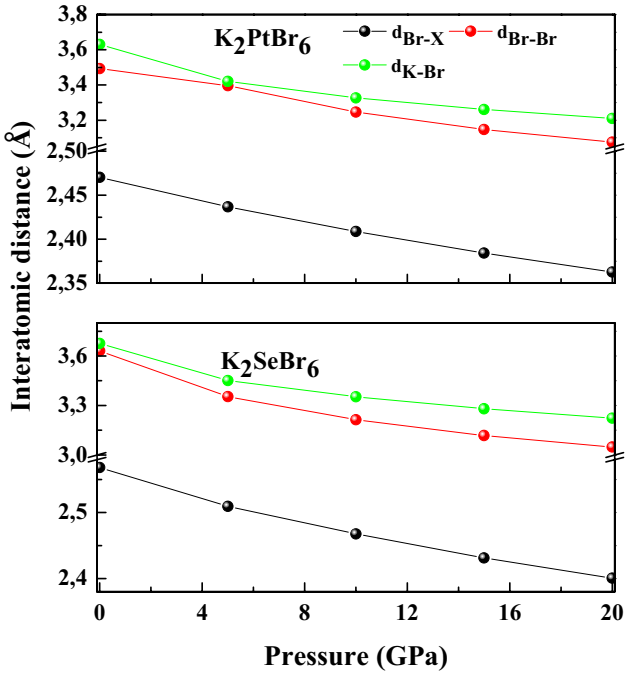

Figure 3. Effect of pressure on bond lengths $d_{K\text{-}Br}$, $d_{Br\text{-}Br}$ and $d_{Br\text{-}X(X=Se,\ Pt)}$ in K_2SeBr_6 and K_2PtBr_6.

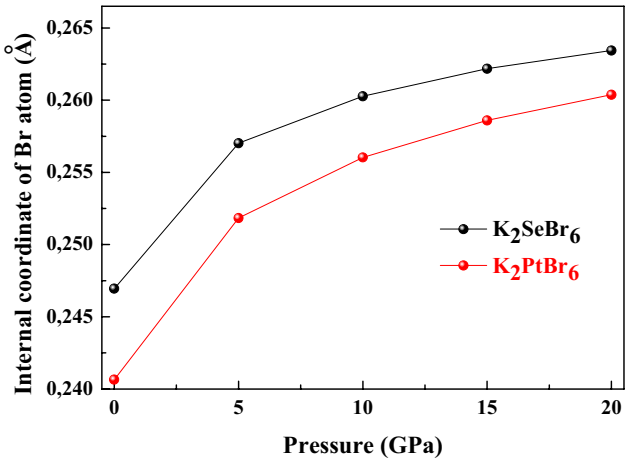

Figure 4. The pressure effect on internal coordinate of Br atom in K_2SeBr_6 and K_2PtBr_6.

Elastic constants and related parameters. The knowledge of elastic constants is essential for a better theoretical understanding of the properties of materials that are determined by the phonons density of states and the electron–phonon interaction processes. The three independent elastic constants C_{11}, C_{12} and C_{44} require for their elastic characterization. The elastic moduli of K_2XBr_6(X = Se, Pt) computed at equilibrium using GGA-PBESOL are reported in Table 1. No theoretical value is reported in the literature, then our computation is prediction. The elastic constants of K_2SeBr_6 and K_2PtBr_6 are significantly small because of their quite large reticular distances, low Colombian forces, so they are quite soft and tolerant to damage. This result is qualitatively explained in these two materials by their binding forces, which are mainly ionic. It was noted that C_{11}, C_{12} and C_{44} agree reasonably with their experiment values[1]. The elastic stability of K_2SeBr_6 and K_2PtBr_6 was defined taking into account the Born's criteria, from which the following conditions must be satisfied for zinc blend structure[18]:

$$0\langle C_{11} + 2C_{12},\ 0\langle C_{44},\ 0\langle C_{11} - C_{12},\ C_{12}\langle C_{11} \tag{1}$$

The bulk modulus calculated from the elastic constants is identical to that deduced from equation of state fitting $P(V/V_0)$. This makes our results as reliable. Figure 5 visualizes the dependence on pressure of K_2XBr_6(X = Se, Pt) elastic moduli. It is observed that the elastic values of GGA-PBESOL increase as a function of the applied

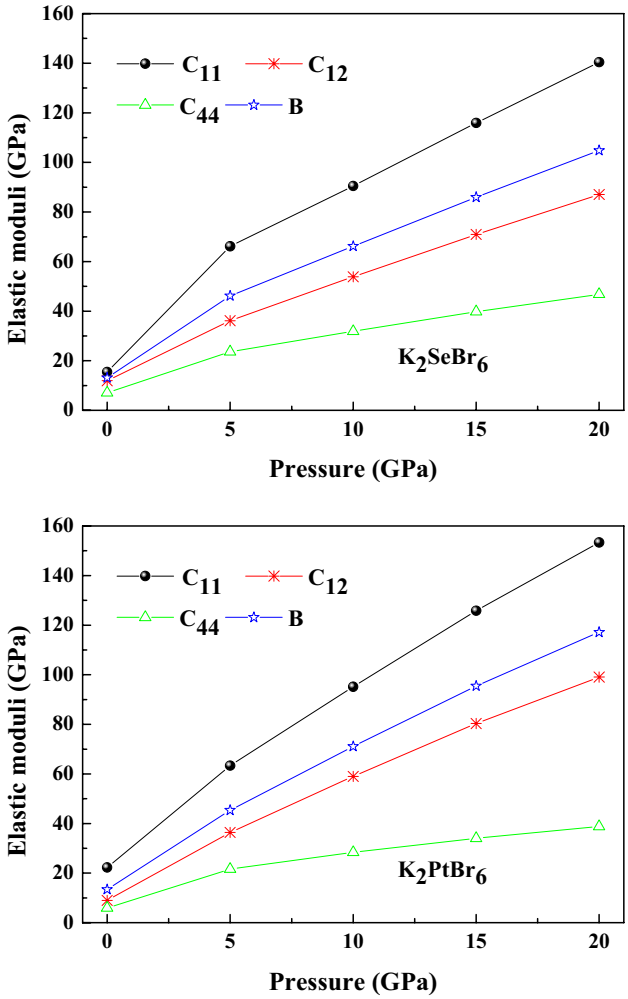

Figure 5. Elastic moduli of K_2SeBr_6 and K_2PtBr_6.

Material	Young'smodulus		Linear compressibility		Shear modulus		Poisson's ratio	
	E_{min}	E_{max}	$^{\beta}$min	$^{\beta}$max	G_{min}	G_{max}	$^{\sigma}$ min	$^{\sigma}$ max
K_2SeBr_6	5.0801	18.014	25.374	25.374	1.7694	7.0839	0.22305	0.94375
K_2PtBr_6	15.565	17.117	24.857	24.857	5.9567	6.6484	0.26729	0.33683

Table 2. The extreme values of Young's modulus (GPa), linear compressibility (GPa), shear modulus (GPa) and Poisson's ratio for K_2XBr_6(X = Pt, Se).

pressure, from zero to 20 GPa. These compounds show weaker elastic constants, which explain their lower hardness. The bulk modulus, shear modulus, Young's modulus, Poisson's ratio, the universal anisotropy and B_H/G_H ratio for isotropic polycrystalline materials of K_2XBr_6(X = Pt, Se) using theVoigt-Reuss-Hill approximation[19–21] are reported in Table 2. The values of the Poisson coefficient between 0.25 and 0.5 are associated with the interatomic forces of central types and covalent bonding character. The nature of the bonds in a compound is described by the factor σ, either ionic-covalent ($0.16 \le \sigma \le 0.30$) in K_2PtBr_6 (0.29) and metallic ($\sigma \ge 0.33$) in K_2SeBr_6 (0.35). The Pugh's criterion (B_H/G_H) and universal anisotropy indicate that K_2XBr_6(X = Pt, Se) are ductile and anisotropic. The extreme values of Young's modulus, linear compressibility, shear modulus and Poisson's ratio for K_2XBr_6(X = Pt, Se) are listed in Table 3. These values prove the isotropic linear compressibility and confirm the anisotropy of the other parameters and the anisotropy is more pronounced in K_2SeBr_6. We represent in Fig. 6 using ELATE software[22] the effect of orientation on mechanical parameters for K_2PtBr_6. Young's modulus, shear modulus and Poisson's ratio are anisotropic, while linear compressibility is isotropic.

Band structure and states densities. Understanding the band structure and estimating band gap of K_2XBr_6(X = Pt, Se), we use both GGA (PBE-SOL) and HSE hybrid functional as shown in Fig. 7. The calcula-

Material	B (GPa)			(GPa)			E_H (GPa)	σ_H	$_AU$	B_H/G_H
	B_V	B_R	B_H	G_V	G_R	G_H				
K_2SeBr_6	13.137	13.137	13.137	4.9581	3.2179	4.088	11.111	0.35903	2.70401	3.21
K_2PtBr_6	13.41	13.41	13.41	6.2334	6.2154	6.2244	16.171	0.29902	0.0145	2.15

Table 3. The bulk modulus, shear modulus, Young's modulus, Poisson's ratio, anisotropy factorand B_H/G_Hratio for K_2XBr_6(X = Pt, Se).

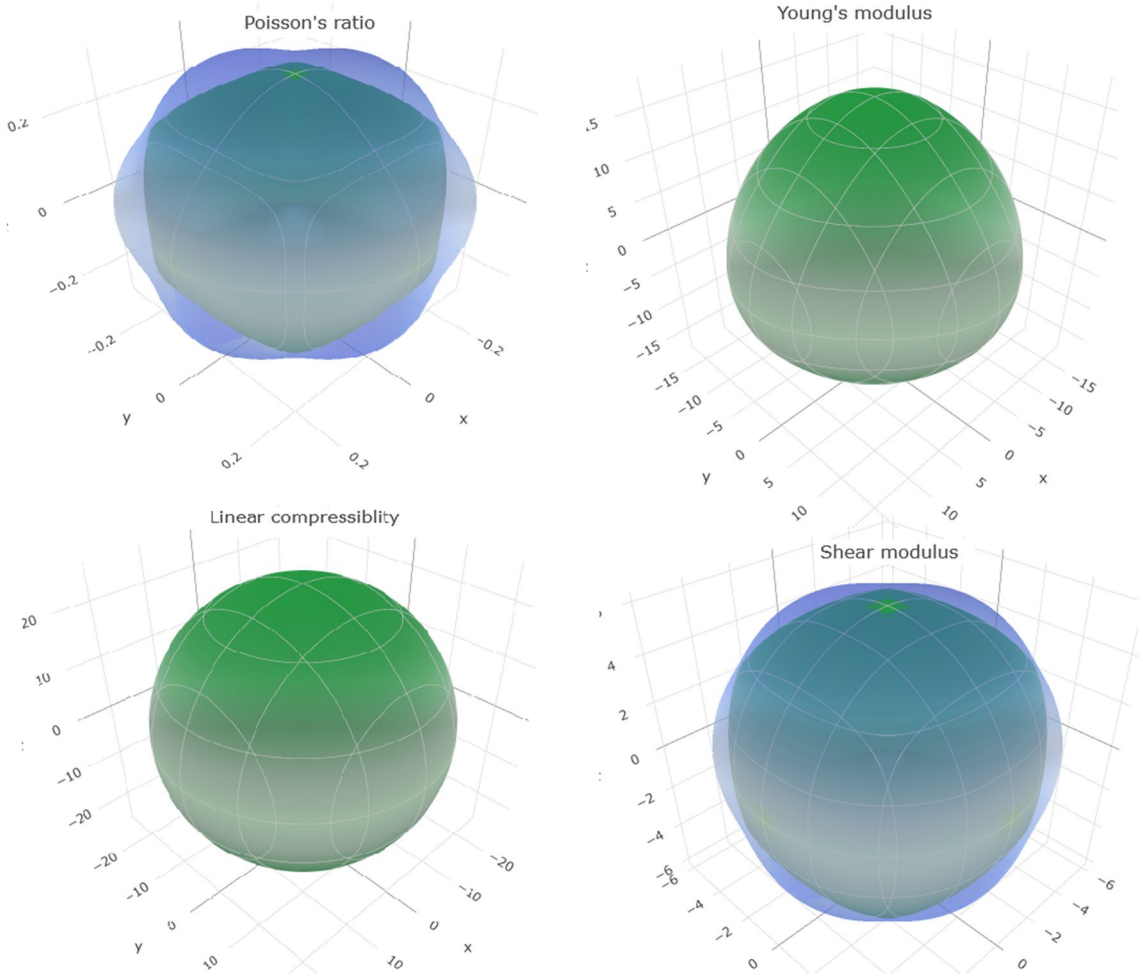

Figure 6. The orientation effect on Poisson's ratio, Young's modulus, linear compressibility and shear modulus in K_2PtBr_6.

tions were conducted on K_2XBr_6(X = Pt, Se), by neglecting the presence of the K-state in the (Pt, Se) site. The electronic band structure of K_2SeBr_6 and k_2PtBr_6 were computed using the equilibrium lattice constant. The bottom of the conduction band is at Γ point for K_2SeBr_6 and k_2PtBr_6. The top of the valence band is at L and X points in K_2SeBr_6 and k_2PtBr_6 compounds, which indicate an indirect band gap Γ-L (Γ-X) of 1.5089 eV and 2.250 eV (0.9818 eV and 1.531 eV) for K_2SeBr_6 (k_2PtBr_6). No experimental and theoretical value are present in the literature, and then our results are predictions. Note that the HSE approximation gives a value close to the experimental one. We report the various band gaps at equilibrium lattice constant for K_2SeBr_6 and k_2PtBr_6 using GGA and HSE in Table 4. By varying the applied pressure between 0 and 20 GPa, the fundamental band gap as shown in Fig. 8 decreases. K_2PtBr_6 becomes metallic at a pressure of 15 GPa. We visualize the plots of PDOS and TDOS of K_2SeBr_6 and K_2PtBr_6 in Fig. 9. The top of valence band region is −2.86 eV to E_F (−2 eV to E_F) for K_2SeBr_6 (k_2PtBr_6). The electronic contribution in this region is due mainly to Br: p orbital in K_2SeBr_6 and K_2PtBr_6. The first conduction band of K_2SeBr_6 (K_2PtBr_6) starts at 1.68 eV (4 eV), then the transitions occur between Br: p and K: p sites. It is noted that the Pt site does not participate in the electronic contribution at the conduction and valence bands.

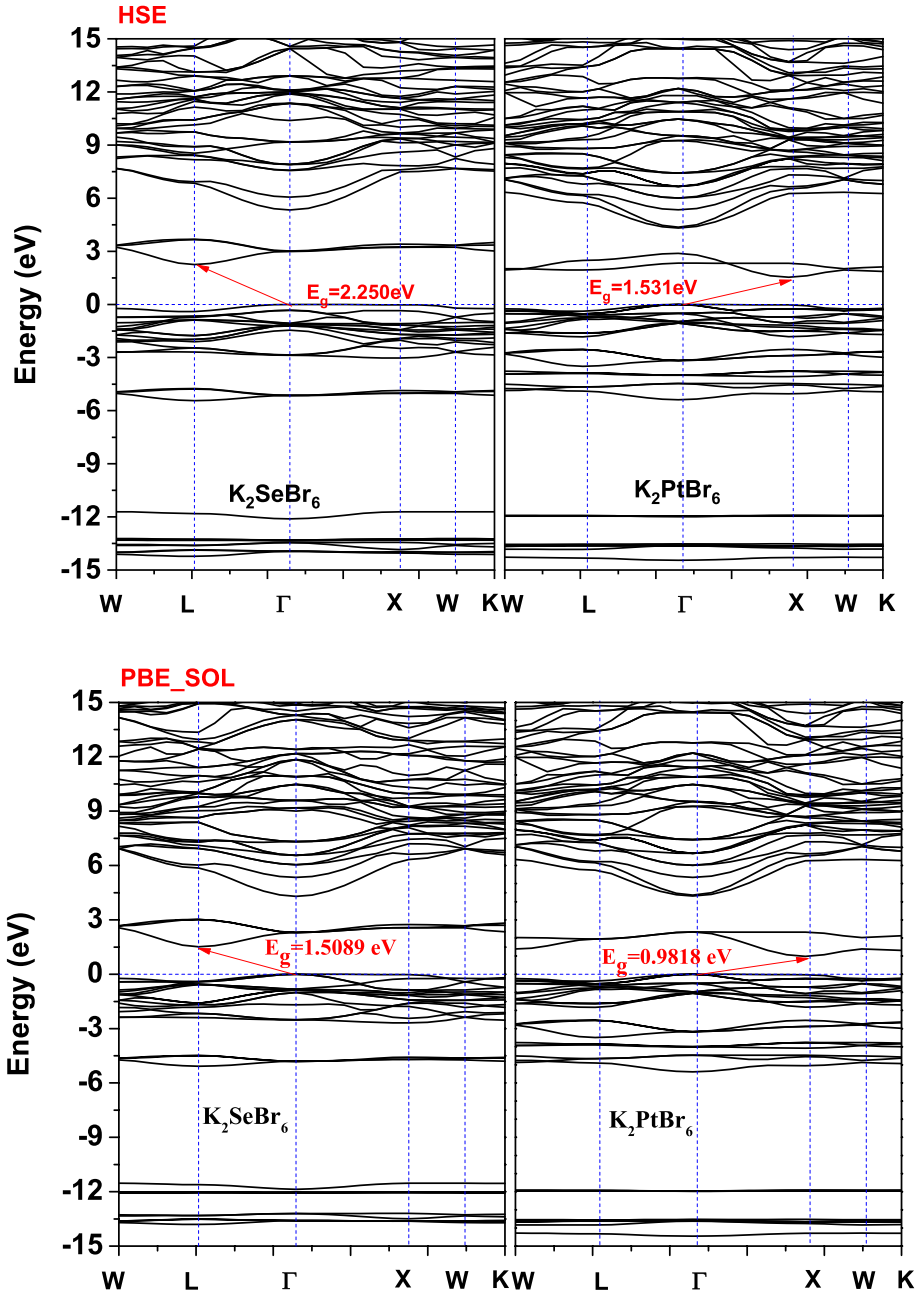

Figure 7. Band structures of K_2XBr_6(X = Pt, Se) in zinc blend structure performed with GGA (PBE-SOL) and HSE hybrid.

Material	EΓ-Γ	EΓ-X	EΓ-L	EX-X	EL-L
K_2PBr_6					
E_0 (eV)	2.323	0.98	1.88	1.14	2.31
$\alpha \times 10^{-2}$ (eV/GPa)	−9.94				
$\beta \times 10^{-3}$ (eV/GPa^2)	2.8				
K_2SeBr_6					
E_0 (eV)	2.29	2.56	1.5	2.58	1.902
$\alpha \times 10^{-2}$ (eV/GPa)	−7.09				
$\beta \times 10^{-3}$ (eV/GPa^2)	1.56				

Table 4. The various band gaps at zero pressure for K_2SeBr_6 and K_2PtBr_6.

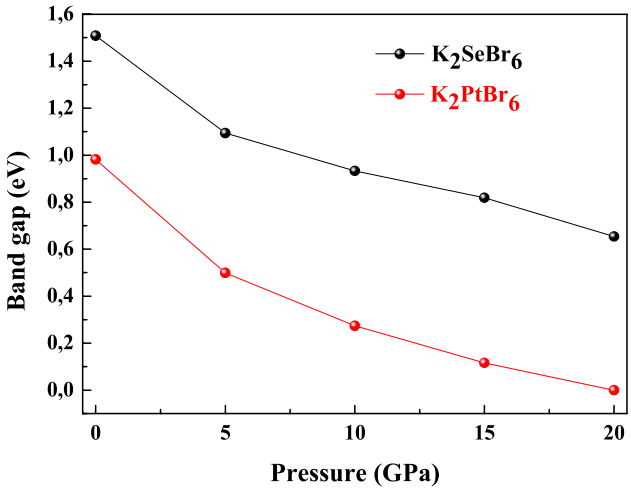

Figure 8. Fundamental band gap of K_2XBr_6(X = Pt, Se) with GGA (PBE-SOL) and HSE hybrid.

Optical properties. The real dielectric constant is a measure of polarization, while the imaginary part is a measure of the dielectric losses. The complex dielectric function is the sum of real and imaginary parts.

$$\varepsilon(\omega) = \varepsilon_1(\omega) + i\varepsilon_2(\omega)$$

The optical quantities such as reflectivity, absorption, loss function and refractive index depend on the structure of the material. These parameters cited above are isotropic in a material with cubic structure. The reflectivity of any material is calculated by dielectric function through the equation:

$$R(\omega) = \left| \frac{(\varepsilon_1)^{1/2} - 1}{(\varepsilon_1)^{1/2} + 1} \right| \tag{2}$$

We display the plots of reflectivity, absorption and loss function as a function of wavelength for K_2SeBr_6 and K_2PtBr_6 in Fig. 10. The reflectivity is a measure of the ability of a material to reflect radiation. The reflectivity of K_2SeBr_6 and K_2PtBr_6 starts at wavelength around 60 nm and reaches several peaks of maxima (0.23) and minima (0.05) in the field of extreme ultraviolet light. In practice, the roughness, uniformity of thickness, inter diffusion, oxidation and thermal stability limit the reflectivity. We observe various absorption peaks in extreme ultraviolet light. These peaks are due to the electronic transitions from the top of the valence band to the bottom of the conduction band. The maximum absorption is between 234,720 cm^{-1} and 229,405 cm^{-1} at wavelength range 56 nm to 105 nm for K_2SeBr_6 and K_2PtBr_6. Indeed, K_2SeBr_6 and K_2PtBr_6 have a narrow gap and absorb extreme ultraviolet light and consequently, they are candidates in the fields of photo catalysis and photovoltaic. The loss function is calculated through the equation:

$$L(\omega) = \frac{\varepsilon_2(\omega)}{\varepsilon_1^2(\omega) + \varepsilon_2^2(\omega)} \tag{3}$$

The loss function demonstrates the existence of two major plasmonic processes, with intensity 3.7 and 1.35 located around 53.5 nm and 72.8 nm. There is no loss in the ultra violet and visible light domains. We present in Fig. 11 the refractive index of K_2SeBr_6 and K_2PtBr_6 as a function of energy. The static refractive index is 2.583 (2.407) for K_2SeBr_6 (K_2PtBr_6). It reaches a series of maxima 3.106 (2.678) and minima 0.383 (0.485) between 1.7 eV and 23 eV for K_2SeBr_6 (K_2PtBr_6). It is reported that an experimental refractive index 2.15 and 2.11 for K_2SeBr_6 and K_2PtBr_6 calculated by N. Wruk et al.[1]. The refractive index is given as:

$$n(\omega) = \frac{\sqrt{2}}{2}\left[\varepsilon_1 + \sqrt{\varepsilon_1^2 + \varepsilon_2^2}\right] \tag{4}$$

The refractive index is more important when photons move through the material and when bonds between atoms are covalent. The static refractive index enhanced with the expansion of the electronic cloud and the increase in density on the structure. The general trend is that the decrease in reflectivity results from the increase

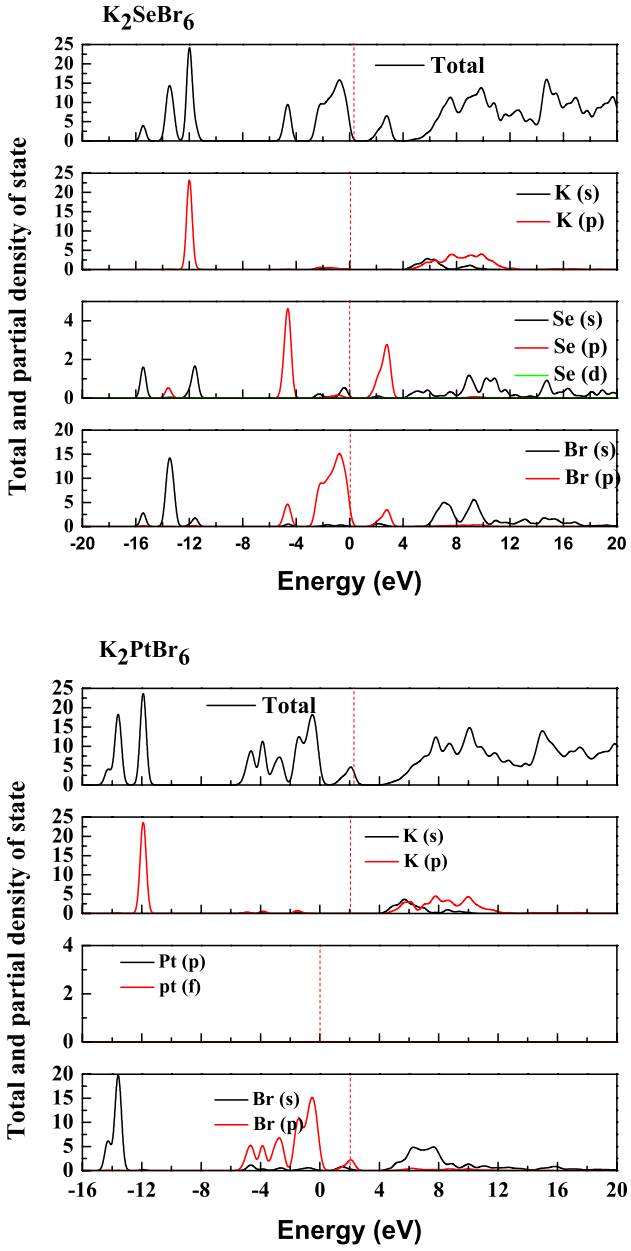

Figure 9. Total and partial density of states for K_2SeBr_6 and K_2PtBr_6.

in absorption and the decrease in refractive index. The plots of imaginary part and $E(k) = E_{Cj}(k) - E_{Vi}(k)$ for K_2SeBr_6(X = Se, Pt) are reported in Fig. 12 (right and left panel). The imaginary part and optical transitions are connected to the absorption coefficient. The main contribution to the optical transitions from six top valence bands to seven lower conduction bands for K_2SeBr_6(X = Se, Pt) are reported in Table 5. The isotropic optical parameters of K_2SeBr_6 and K_2PtBr_6 makes them as windows and lenses. The band gap range (1–2.25 eV) and absorption of extreme ultraviolet light make K_2SeBr_6 and K_2PtBr_6 as absorber materials.

Conclusion

Employing a plane-wave pseudo-potential using the DFT framework, within the generalized gradient approximation, we studied the structural, mechanical and optoelectronic parameters of K_2PtBr_6 and K_2SeBr_6 hexahalometallate materials. The bulk modulus of K_2SeBr_6 and K_2PtBr_6 agrees well with experiment value where the error

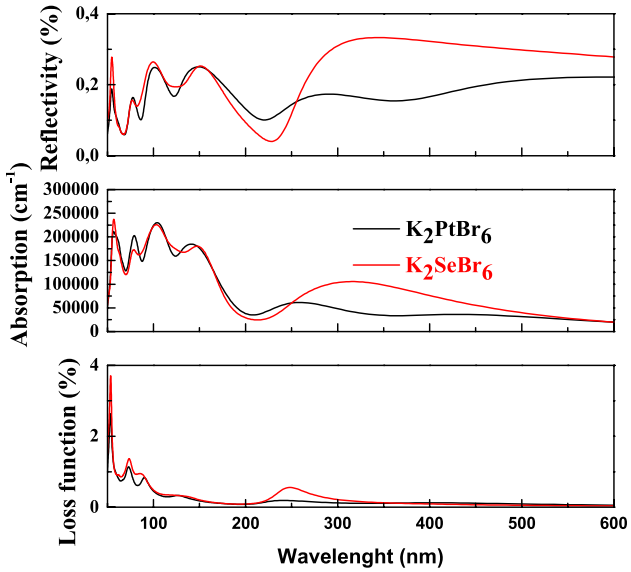

Figure 10. The reflectivity, absorption and loss function in K_2SeBr_6 and K_2PtBr_6.

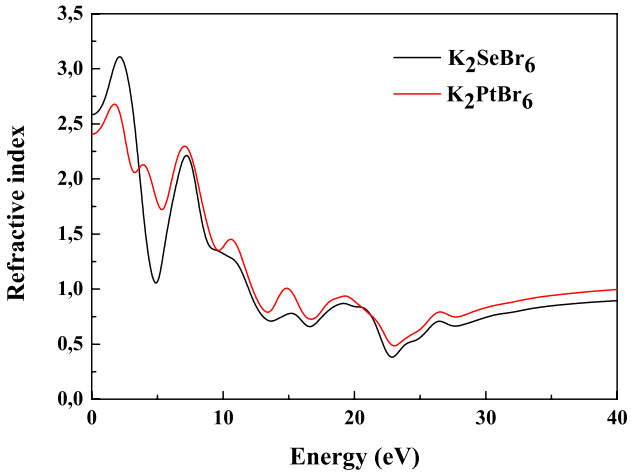

Figure 11. The refractive index in K_2SeBr_6 and K_2PtBr_6.

is 8% and 1.4%. The elastic constants of K_2SeBr_6 and K_2PtBr_6 are significantly smaller, then they are fairly soft and damage tolerant. An electronic study shows that K_2PtBr_6 is indirect band gap semiconductor and becomes metallic at a pressure of 15 GPa. The partial density of states indicates that the valence electrons are transferred from Br: p state to K: p site. The band gap size, optical absorption and reflectivity make K_2SeBr_6 and K_2PtBr_6 as candidate absorbers. The static refractive index increases with the expansion of the electronic cloud and the increase in density on the structure. The general trend is that the decrease in reflectivity results from the increase in absorption and the decrease in refractive index. There is no loss in the ultra violet and visible light domains. The compounds are poor reflector and can be used as an anti-reflection coating material.

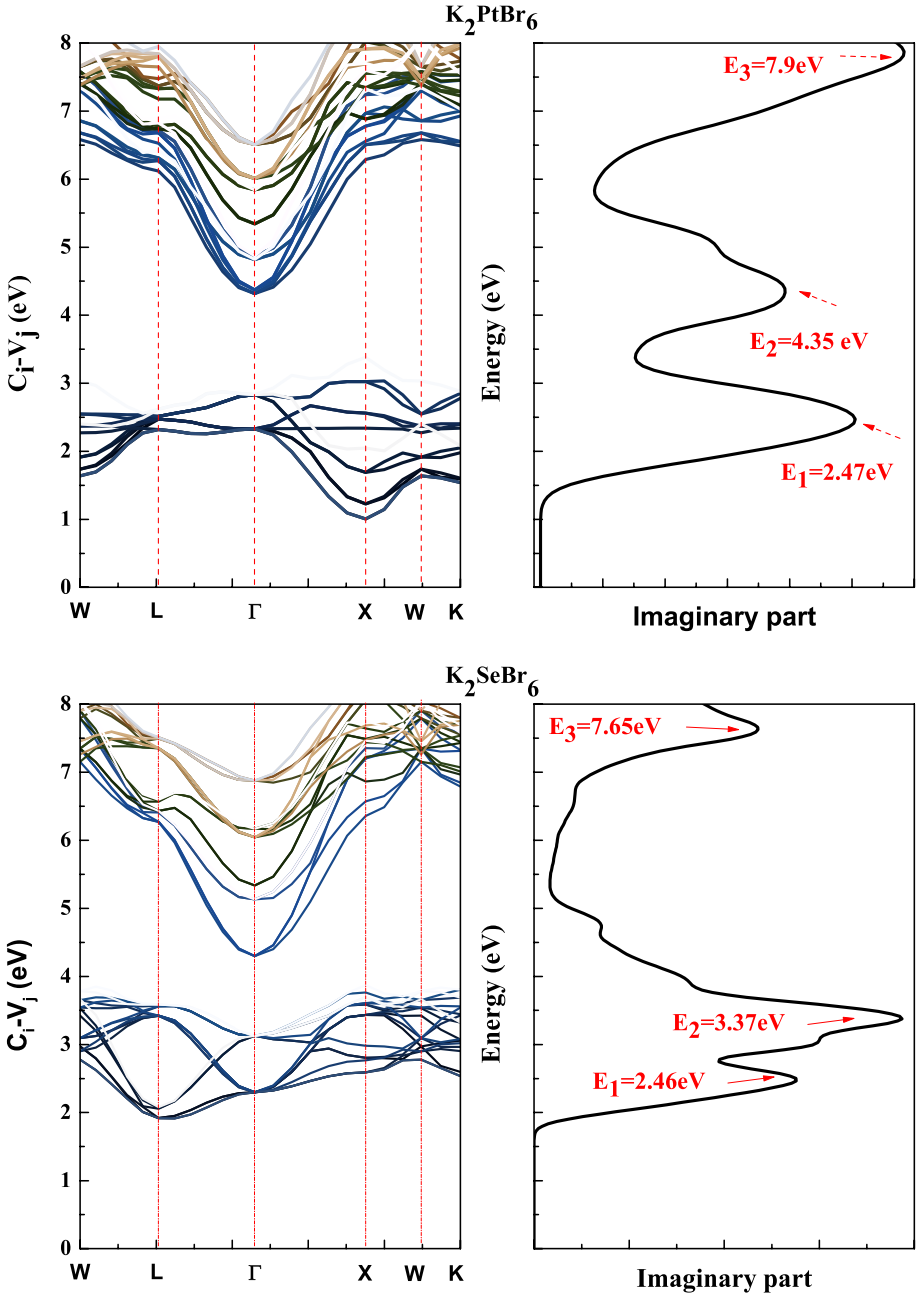

Figure 12. The imaginary part and transition energy in K_2SeBr_6 and K_2PtBr_6.

Peaks	$W \rightarrow L$	$L \rightarrow \Gamma$	$\Gamma \rightarrow X$	$X \rightarrow W$	$W \rightarrow K$
K_2PtBr_6					
$E = 2.47\ eV$	$V_5 \rightarrow C_2$, $V_3 \rightarrow C_2$ $V_4 \rightarrow C_1$, $V_6 \rightarrow C_1$		$V_5 \rightarrow C_1$	$V_3 \rightarrow C_2$	
$E = 4.35\ eV$		$V_3 \rightarrow C_3$, $V_1 \rightarrow C_4$, $V_1 \rightarrow C_3$			
$E = 7.9\ eV$	$V_3 \rightarrow C_4$, $V_4 \rightarrow C_4$ $V_5 \rightarrow C_4$	$V_6 \rightarrow C_7$, $V_6 \rightarrow C_5$ $V_5 \rightarrow C_7$, $V_5 \rightarrow C_6$	$V_6 \rightarrow C_7$, $V_5 \rightarrow C_7$ $V_6 \rightarrow C_6$, $V_3 \rightarrow C_6$ $V_3 \rightarrow C_5$, $V_1 \rightarrow C_6$		
$E = 7.47\ eV$	$V_6 \rightarrow C_7$		$V_6 \rightarrow C_7$, $V_4 \rightarrow C_7$ $V_3 \rightarrow C_7$		
K_2SeBr_6					
$E = 2.46\ eV$	$V_1 \rightarrow C_1$, $V_6 \rightarrow C_1$, $V_3 \rightarrow C_1$	$V_5 \rightarrow C_1$, $V_1 \rightarrow C_2$ $V_3 \rightarrow C_3$	$V_1 \rightarrow C_1$		
$E = 3.35\ eV$	$V_3 \rightarrow C_3$, $V_5 \rightarrow C_1$, $V_1 \rightarrow C_3$, $V_3 \rightarrow C_3$	$V_5 \rightarrow C_2$, $V_3 \rightarrow C_6$, $V_3 \rightarrow C_4$	$V_6 \rightarrow C_1$	$V_3 \rightarrow C_2$	
$E = 7.65\ eV$	$V_5 \rightarrow C_3$, $V_6 \rightarrow C_6$ $V_6 \rightarrow C_7$, $V_4 \rightarrow C_6$ $V_5 \rightarrow C_7$	$V_6 \rightarrow C_7$, $V_6 \rightarrow$ C_5 $V_5 \rightarrow C_7$, $V_6 \rightarrow C_4$	$V_6 \rightarrow C_7$, $V_3 \rightarrow C_7$ $V_6 \rightarrow C_5$, $V_2 \rightarrow C_7$ $V_6 \rightarrow C_5$	$V_6 \rightarrow C_4$, $V_5 \rightarrow C_2$	

Table 5. The main contribution to the optical transitions for K_2SeBr_6(X = Se, Pt).

Received: 4 January 2022; Accepted: 28 April 2022
Published online: 18 May 2022

References

1. Wruk, N., Pelzl, J., Saundersn, G. A. & Hailing, T. *J. Phys. Chem. Solids* **46**(11), 1235–1242 (1985).
2. Abriel, W. & White, M. A. *J. Chem. Phys.* **93**, 8321 (1990).
3. Eperon, G. E. *et al. J. Mater. Chem. A* **3**(39), 19688–19695. https://doi.org/10.1039/C5TA06398A (2015).
4. Green, M. A., Ho-Baillie, A. & Snaith, H. J. *Nat. Photonics* **8**(7), 506–514. https://doi.org/10.1038/nphoton.2014.134 (2014).
5. Kojima, A., Teshima, K., Shirai, Y. & Miyasaka, T. *J. Am. Chem. Soc.* **131**, 6050–6051 (2009).
6. Yin, W. J., Shi, T. & Yan, Y. *Adv. Mater.* **26**, 4653–4658 (2014).
7. Huang, X., Paudel, T. R., Dowben, P. A., Dong, S. & Tsymbal, E. Y. *Phys. Rev. B* **94**, 195309 (2016).
8. Clark, S. J. *et al. Zeitschrift Fur Kristallographie.* **220**, 567–570. https://doi.org/10.1524/zkri.220.5.567.65075 (2005).
9. Vanderbilt, D. *Phys. Rev. B* **41**, 7892 (1990).
10. Perdew, J. P., Burke, K. & Ernzerhof, M. *Phys. Rev. Lett.* **77**, 3865 (1996).
11. Monkhorst, H. J. & Pack, J. D. *Phys. Rev. B* **13**, 5188 (1976).
12. Fischer, T. H. & Almlof, J. *J. Phys. Chem.* **96**, 9768 (1992).
13. Marti, D., Dupertuis, M.-A. & Deveaud, B. General theory for the interference of two-photon and one-photon processes in semiconductor heterostructures. *Ann. Phys.* **316**, 234 (2005).
14. Pickard, C. J. & Payne, M. C. Second-order kp perturbation theory with Vanderbilt pseudopotentials and plane waves. *Phys. Rev. B* **62**, 4383 (2000).
15. GajdoS, M., Hummer, K., Kresse, G., Furthmüller, J. & Bechstedt, F. Linear optical properties in the projector-augmented wave methodology. *Phys. Rev. B* **73**, 045112 (2006).
16. Magdalena Laurien, Oleg Rubel, Cond-mat. mtrl-sci (2021).
17. Read, A. J. & Needs, R. J. Calculation of optical matrix elements with nonlocal pseudopotentials. *Phys. Rev. B* **44**, 13071 (1991).
18. Sinko, G. V. & Smirnov, N. A. *J. Phys.: Condens. Matter* **14**, 6989 (2002).
19. Voigt, W. *Lehrbuch der Kristallphysik* (Teubner, 1928).
20. Reuss, A. & Angew, Z. *Math. Mech.* **9**, 49–58 (1929).
21. Hill, R. *Proc. Phys. Soc. London A* **65**, 349 (1952).
22. Gaillac, R., Pullumbi, P. & Coudert, F.-X. ELATE: an open-source online application for adnalysis and visualization of elastic tensors. *J. Phys. Condens. Matter* **28**, 275201. https://doi.org/10.1088/0953-8984/28/27/275201 (2016).

Acknowledgements

We would like to thank Taif University Research Supporting Project number (TURSP-2020/63), Taif University, Taif, Saudi Arabia.

Author contributions

Manuscript title:Fundamental properties of hexahalometallate single crystals K2XBr6(X= Se, Pt): Ab initio study. All authors who have made substantial contributions to the work reported in the manuscript .the role of each author in the paper.• Conceptualization , Data curation, Formal analysis: a-c• Investigation, Methodology, Project administration, Resources: c - e• Software, Supervision, Validation, Visualization, Writing - original draft, Writing - review editing: c, f.This statement is approved by all the authors.

Competing interests

The authors declare no competing interests.

Additional information

Correspondence and requests for materials should be addressed to M.F.